Inorg. Chem. **2008**, *47*, 8511−8517

Forum

Polar Hexagonal Tungsten Bronze-Type Oxides: $KNbW_2O_9$, $RbNbW_2O_9$, and $KTaW_2O_9$

H. Y. Chang,[†] T. Sivakumar,[†,‡] K. M. Ok,[§] and P. Shiv Halasyamani*[,†]

Department of Chemistry, University of Houston, 136 Fleming Building, Houston, Texas 77204-5003, and Department of Chemistry, Chung-Ang University, 221 Heukseok-dong, Dongjak-gu Seoul 155-756, Korea

Received March 31, 2008

The synthesis, crystal structures, second-harmonic generation (SHG), piezoelectric, pyroelectric, and ferroelectric properties of three polar noncentrosymmetric (NCS) hexagonal tungsten bronze-type oxides are reported. The materials $KNbW_2O_9$, $RbNbW_2O_9$, and $KTaW_2O_9$ were synthesized by standard solid-state techniques and structurally characterized by laboratory powder X-ray diffraction. The compounds are isostructural, crystallizing in the polar NCS space group *Cmm*2. The materials exhibit a corner-shared MO_6 (M = Nb^{5+}/W^{6+} or Ta^{5+}/W^{6+}) octahedral framework, with K^+ or Rb^+ occupying the "hexagonal" tunnels. The d^0 transition metals, Nb^{5+}, Ta^{5+}, and W^{6+}, are displaced from the center of their oxide octahedra attributable to second-order Jahn−Teller effects. SHG measurements using 1064 nm radiation revealed frequency-doubling efficiencies ranging from 180 to 220 × α-SiO_2. Converse piezoelectric measurements resulted in d_{33} values ranging from 10 to 41 pm V^{-1}. The total pyroelectric coefficient, *p*, at 50 °C ranged from −6.5 to −34.5 μC K^{-1} m^{-2}. The reported materials are also ferroelectric, as demonstrated by hysteresis loops (polarization vs electric field). Spontaneous polarization values, P_s, ranging from 2.1 to 8.4 μC cm^{-2} were measured. The magnitudes of the SHG efficiency, piezoelectric response, pyroelectric coefficient, and ferroelectric polarization are strongly dependent on the out-of-center distortion of the d^0 transition metals. Structure−property relationships are discussed and explored. Crystal data: $KNbW_2O_9$, orthorhombic, space group *Cmm*2 (No. 35), *a* = 21.9554(2) Å, *b* = 12.60725(15) Å, *c* = 3.87748(3) Å, *V* = 1073.273(13) $Å^3$, and *Z* = 6; $RbNbW_2O_9$, orthorhombic, space group *Cmm*2 (No. 35), *a* = 22.00985(12) Å, *b* = 12.66916(7) Å, *c* = 3.8989(2) Å, *V* = 1086.182(10) $Å^3$, and *Z* = 6; $KTaW_2O_9$, orthorhombic, space group *Cmm*2 (No. 35), *a* = 22.0025(2) Å, *b* = 12.68532(14) Å, *c* = 3.84456(4) Å, *V* = 1073.05(2) $Å^3$, and *Z* = 6.

Introduction

The design and synthesis of compounds to exhibit specific functional properties remains a challenge for chemists. This is unquestionably the situation with polar materials, i.e., compounds that have a permanent dipole moment. In molecular systems, H_2O, HCl, NH_3, etc., the concept of the dipole moment is rather straightforward: the dipole moment is directed from the electropositive element toward the electronegative element. In compounds that exhibit extended structures, metal oxides for example, polarity is slightly more complicated. For a solid-state material to be considered polar, the compound must crystallize in 1 of 10 crystal classes: 1, 2, 3, 4, 6, *m*, *mm*2, 3*m*, 4*mm*, or 6*mm*.[1] Within each of these crystal classes, there are specifically defined polar directions.[1] Materials exhibiting polarity have the correct symmetry for four specific functional materials properties: second-harmonic generation (SHG), piezoelectricity, pyroelectricity, and fer-

* To whom correspondence should be addressed. E-mail: psh@uh.edu.
† University of Houston.
‡ Current address: Department of Chemistry, University of New Orleans, New Orleans, LA 70148.
§ Chung-Ang University.

(1) Hahn, T. *Internationa Tables for Crystallography, Volume A, Space Group Symmetry*; Kluwer Academic: Dordrecht, Holland, 2006; Vol. *A*.

10.1021/ic800573k CCC: $40.75
Published on Web 09/29/2008

roelectricity.[2,3] With SHG and piezoelectricity, polarity is not required, whereas for pyroelectricity and ferroelecitricy, the material in question must be polar. All four phenomena have been discussed extensively in the literature,[4−7] so only a brief description will be given here.

SHG. SHG, or frequency doubling, can be defined as the conversion of a specific wavelength of light into half of its original, i.e., $\lambda_1 \rightarrow {}^1/_2\lambda_1$, or with respect to frequency ω, $\omega_1 \rightarrow 2\omega_1$. Not until the invention of the laser by Maiman in 1960[8] could sizable nonlinear optical effects, such as SHG, be observed. The induced polaritzation attributable to the large optical fields, P, that is observed can be written as a power series: $P = \chi E + dE^2 + ...$, where χ is the linear electric susceptibility, with the higher order terms leading to nonlinear effects such as SHG. These nonlinear effects are described by expanding the polarization:

$$P_i = \chi_{ij}E_j + \chi_{ijk}E_jE_k + \chi_{ijkl}E_jE_kE_l + ...$$

where χ_{ij} is the electric susceptibility and χ_{ijk} is the second-order nonlinear coefficient. It is only in a noncentrosymmetric (NCS) environment that $\chi_{ijk} \neq 0$. In experimental SHG measurements, χ_{ijk} is replaced by d_{ijk} coefficients, where $2d_{ijk} = \chi_{ijk}$. After the invention of the laser, SHG was first observed in large single crystals of quartz in 1961 by Franken et al.[9] For several years following Franken's result, large single crystals (several *mm*) were required to measure SHG. A technique that used polycrystalline samples was described in 1968[10] and thereby removed the need for large crystals. With this technique, the SHG efficiency and the type 1 phase-matching behavior of the material may be determined. Type 1 phase matching, or index matching, occurs when the phase velocity of the fundamental radiation (1064 nm) equals the second harmonic (532 nm). If type 1 phase matching occurs, the SHG efficiency will increase with the particle size and plateau at a maximum value. If phase matching does not occur, the SHG efficiency will reach a maximum value and then decrease, as the particle size increases. Particle sizes used are between 20 and 150 μm. Once the phase-matching capabilities of the material are known, the bulk nonlinear optical susceptibility, $\langle d_{\text{eff}} \rangle$, can be estimated. The values of $\langle d_{\text{eff}} \rangle$ for phase-matchable and non-phase-matchable materials are as follows:

$$\langle d_{\text{eff}} \rangle_{\text{PM}} = \left\{ \frac{I^{2\omega}(\text{A})}{I^{2\omega}(\text{LiNbO}_3)} \times 7.98 \times 10^2 \right\}^{1/2}$$

$$\langle \text{d}_{\text{eff}} \rangle_{\text{NPM}} = \left\{ \frac{I^{2\omega}(\text{A})}{I^{2\omega}(\text{SiO}_2)} \times 0.3048 \right\}^{1/2}$$

The SHG efficiency of the unknown compound (A) is compared with either $LiNbO_3$ (SHG efficiency of 600 × SiO_2) or SiO_2 depending on whether the material is phase-matchable (PM) or non-phase-matchable (NPM). The units for $\langle d_{\text{eff}} \rangle$ are picometers per volt (pm V^{-1}).

Piezoelectricity. Piezoelectricity was discovered in 1880 by Jacques and Pierre Curie.[11] They observed that some materials become electrically polarized when subjected to a mechanical force. Soon after the converse effect was described, wherein the application of a voltage produced a macroscopic strain. With the direct effect, an external stress, σ_{jk}, results in a change in polarization, P_i, and is formulated as $P_i = d_{ijk}\sigma_{jk}$, where d_{ijk} ($i, j, k = 1, 2, 3$) is the piezoelectric charge coefficient, given in coulombs per newton (C N^{-1}). With the converse effect, an applied field, E_i, results in a strain, ϵ_{jk}, and is formulated as $\epsilon_{jk} = d_{ijk}E_i$, where d_{ijk} is the piezoelectric strain coefficient, given in meters per volt (m V^{-1}). With both effects, d_{ijk} is a third-rank tensor. It is important to note that the units for d_{ijk} when direct or converse effects are measured are equivalent, that is, 1 C N^{-1} = 1 m V^{-1}. Both direct and converse effects are used in a variety of applications. The direct effect results in generator action: the piezoelectric material converts mechanical energy to electrical energy. This generator action is used in solid-state batteries, sensing devices, and fuel-lighting applications. The converse effect results in motor action: the piezoelectric material converts electrical energy to mechanical energy. This motor action is used in ultrasonic and acoustic applications, micromotor devices, and electromechanical transducers.

Pyroelectricity. The pyroelectric effect may be defined as the change in spontaneous polarization, P_s, as a function of the temperature.[12] The pyroelectric coefficient, **p**, a vector, in units of μC m^{-2} K^{-1}, can be defined as

$$\mathbf{p} = \frac{\text{d}P_s}{\text{d}T}$$

with the spontaneous polarization, P_s, and temperature, T, given in units of μC m^{-2} and K, respectively. Surprisingly, the effect has been known for over 2400 years, with the first account attributed to the Greek philosopher Theophrastus. He described a stone, lyngourion (probably tourmaline), that was capable of attracting straw and pieces of wood. The pyroelectric effect can be subdivided into primary and secondary effects. The primary effect is observed when the material is rigidly clamped under a constant strain to prevent any thermal expansion or contraction. Secondary effects occur when the material is permitted to deform; i.e., the

(2) Nye, J. F. *Physical Properties of Crystals*; Oxford University Press: Oxford, U.K., 1957.
(3) Halasyamani, P. S.; Poeppelmeier, K. R. *Chem. Mater.* **1998**, *10*, 2753.
(4) Cady, W. G. *Piezoelectricity; an Introduction to the Theory and Applications of Electromechanical Phenomena in Crystals*; Dover: New York, 1964; p 822.
(5) Lang, S. B., *Sourcebook of Pyroelectricity*; Gordon & Breach Science: London, 1974.
(6) Lines, M. E.; Glass, A. M., *Principles and Applications of Ferroelectrics and Related Materials*; Oxford University Press: Oxford, U.K., 1991; p 576.
(7) Ok, K. M.; Chi, E. O.; Halasyamani, P. S. *Chem. Soc. Rev.* **2006**, *35*, 710.
(8) Maiman, T. *Br. Commun. Electron.* **1960**, *7*, 674.
(9) Franken, P. A.; Hill, A. E.; Peters, C. W.; Wienrich, G. *Phys. Rev. Lett.* **1961**, *7*, 118.
(10) Kurtz, S. K.; Perry, T. T. *J. Appl. Phys.* **1968**, *39*, 3798.
(11) Curie, J.; Curie, P. *Bull. Soc. Miner. Fr.* **1880**, *3*, 90.
(12) Lang, S. B.; Das-Gupta, D. K. Pyroelectricity: Fundamentals and Applications. In *Handbook of Advanced Electronic and Photonic Materials and Devices*, Nalwa, H. S., Ed.; Academic Press: San Francisco, 2001; Vol. *4*, p 1.

material is under constant stress. Thermal expansion results in a strain that changes the spontaneous polarization attributable to the piezoelectric effect. Thus, the secondary pyroelectric effect includes contributions caused by piezoelectricity. Exclusively measuring the pyroelectric coefficient under constant strain is experimentally very difficult. What is experimentally measured is the total pyroelectric effect exhibited by the material: the sum of the primary and secondary effects. Pyroelectric devices respond to changes in the temperature and therefore can be used to detect and observe stationary or moving objects. A few of the applications for pyroelectric detectors include burglar alarms, pollution monitors, and measurement of the thermal properties of materials.

Ferroelectricity. A ferroelectric may be formally defined as a pyroelectric material that has a reversible, or "switchable", polarization.[6] Thus, the material must be polar, must possess a permanent dipole moment, and must be capable of having this moment reversed in the presence of an applied voltage. The former occurs if the material crystallizes in 1 of 10 polar crystal classes (1, 2, 3, 4, 6, *m*, *mm*2, 3*m*, 4*mm*, or 6*mm*). Determining the latter is more involved. Polarization reversal, or ferroelectric hysteresis, may be measured through a Sawyer−Tower circuit.[13] Additionally, the relatively large voltages needed for polarization reversal require the material under investigation to be insulating. Another feature that is observed in some, but not all, ferroelectric materials is a dielectric anomaly at the Curie temperature. A maximum in the dielectric constant is often observed at the Curie temperature. The circuit design for measuring ferroelectric hysteresis curves was published in 1930.[13] Since that time, there have been a few reports modifying the original design,[14,15] but the overall concept has not changed in over 70 years. At its most basic, a linear capacitor is placed in series with the sample. An ac or dc voltage is then applied. The voltage measured across the capacitor is equivalent to the polarization of the sample. The measurement of spontaneous polarizations on the order of 5−50 μC cm^{-2} in bulk samples requires voltages in excess of 1000 V. The circuit is used to measure a ferroelectric hystersis loop, i.e., the material's switchability in the presence of an applied voltage. The hysteresis loop is determined by measurement of the polarization of the material, in μC cm^{-2}, as a function of the applied voltage or electric field.

Figure 1 presents all four physical properties along with their respective definition, coefficient, and units.

Clearly, polar NCS materials are an important class of compounds. Yet the question remains, how is a polar inorganic material synthesized? We have used d^0 transition metals toward the synthesis of new polar materials.[16−19] In

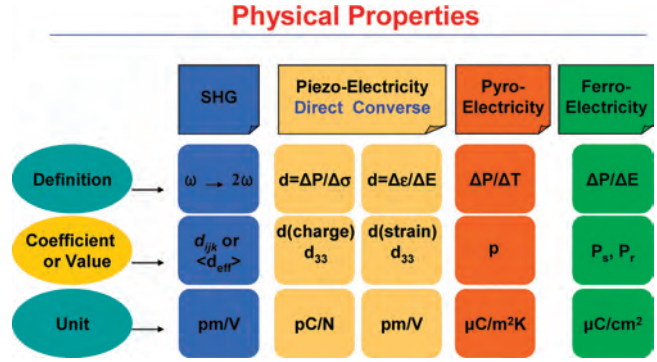

Figure 1. "Acentric" physical properties: SHG, piezoelectricity, pyroelectricity, and ferroelectricity (definitions, coefficients, and units).

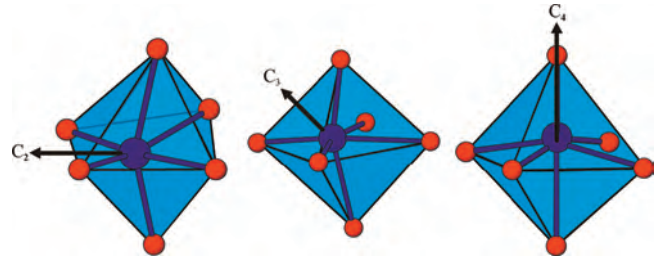

Figure 2. Intraoctahedral distortion of a d^0 cation toward an edge (local C_2), a face (local C_3), and a corner (local C_4).

oxide octahedra, the d^0 transition metals are in an asymmetric coordination environment attributable to second-order Jahn−Teller (SOJT) effects.[20−26] SOJT effects occur when the empty d orbitals of the metal mix with the filled p orbitals of the oxide ligands. In extended structures, this mixing results in a spontaneous distortion of the metal cations that removes the near degeneracy of the p and d orbitals. The d^0 metal distorts from the center of the octahedron toward an edge, face, or vertex.[27] As seen in Figure 2, the resulting geometries are polar with local site symmetries of 1, 2, *mm*2, 3, 3*m*, 4, or 4*mm*. It is this local polarity that is retained in the extended solid-state structure.

One family of materials where polarity can be exploited is in the hexagonal tungsten bronze (HTB) family. The structural archetype may be formulated as A_xWO_3 with $x \sim 0.3$.[28,29] The structure consists of corner-shared WO_6 octahedra that form a hexagonal network, wherein the "A" cation resides. As written, the material is electrically conductive,[29] rendering the material "nonferroelectric". The conductivity can be removed if some of the W^{6+} ions are replaced by cations of lesser valency, e.g., Ti^{4+} or Nb^{5+}. Thus, A_xWO_3 could be reformulated as $A(B^{5+}W^{6+})_3O_9$ or ABW_2O_9, where A = alkali metal and B = Nb^{5+} or Ta^{5+}. With these materials

(13) Sawyer, C. B.; Tower, C. H. *Phys. Rev.* **1930**, *35*, 269.
(14) Dias, E. D.; Pragasam, R.; Murthy, V. R. K.; Viswanathan, B. *Rev. Sci. Instrum.* **1994**, *65*, 3025.
(15) Dawber, M.; Farnan, I.; Scott, J. F. *Am. J. Phys.* **2003**, *71*, 819.
(16) Goodey, J.; Ok, K. M.; Broussard, J.; Hofmann, C.; Escobedo, F. V.; Halasyamani, P. S. *J. Solid State Chem.* **2003**, *175*, 3.
(17) Ra, H. S.; Ok, K. M.; Halasyamani, P. S. *J. Am. Chem. Soc.* **2003**, *125*, 7764.
(18) Chi, E. O.; Gandini, A.; Ok, K. M.; Zhang, L.; Halasyamani, P. S. *Chem. Mater.* **2004**, *16*, 3616.
(19) Chi, E. O.; Ok, K. M.; Porter, Y.; Halasyamani, P. S. *Chem. Mater.* **2006**, *18*, 2070.
(20) Opik, U.; Pryce, M. H. L. *Proc. R. Soc. London, Ser. A* **1957**, *238*, 425.
(21) Bader, R. F. W. *Mol. Phys.* **1960**, *3*, 137.
(22) Bader, R. F. W. *Can. J. Chem.* **1962**, *40*, 1164.
(23) Pearson, R. G. *J. Am. Chem. Soc.* **1969**, *91*, 4947.
(24) Pearson, R. G. *THEOCHEM* **1983**, *103*, 25.
(25) Wheeler, R. A.; Whangbo, M. H.; Hughbanks, T.; Hoffmann, R.; Burdett, J. K.; Albright, T. A. *J. Am. Chem. Soc.* **1986**, *108*, 2222.
(26) Kunz, M.; Brown, I. D. *J. Solid State Chem.* **1995**, *115*, 395.
(27) Goodenough, J. B. *Annu. Rev. Mater. Sci.* **1998**, *28*, 1.
(28) Magneli, A. *Acta Chem. Scand.* **1951**, *5*, 670.
(29) Magneli, A. *Acta Chem. Scand.* **1953**, *7*, 315.

the corner-shared metal−oxide octahedra contain d^0 transition metals that could undergo out-of-center distortions and ideally crystallize in a NCS and polar space group. There have been reports of ABW_2O_9 compounds in the literature,[30−32] as well as spectroscopic studies.[33,34] In these papers, however, there are no definitive crystal structures, i.e., atomic coordinates and bond lengths. We report in this paper the synthesis, crystal structures, and physical property measurements on three polar oxide materials, $KNbW_2O_9$, $RbNbW_2O_9$, and $KTaW_2O_9$. We also discuss structure−property relationships and examine the influence of the d^0 transition metal on the associated physical properties.

Experimental Section

Synthesis. The starting materials were high-purity (>99%) chemicals obtained from Alfa-Aesar. Polycrystalline samples of $KNbW_2O_9$, $RbNbW_2O_9$, and $KTaW_2O_9$ were synthesized by conventional solid-state reactions. Stoichiometric amounts of the corresponding metal nitrate ANO_3 (A = K or Rb), Nb_2O_5 or Ta_2O_5, and WO_3 were thoroughly ground in an agate mortar and pestle and calcined at 900−1000 °C in a platinum crucible for 12−36 h with intermediate grindings. $KNbW_2O_9$, $RbNbW_2O_9$, and $KTaW_2O_9$ were prepared at 900 °C for 24 h, at 920 °C for 24 h, and at 1000 °C for 12 h, respectively. Attempts to prepare the corresponding oxides, $RbTaW_2O_9$, $CsNbW_2O_9$, and $CsTaW_2O_9$, did not yield single-phase products attributable to the formation of pyrochlores.[35,36] The results are consistent with previous studies of A_xWO_3 bronzes that indicated that the pyrochlore structure is stabilized by larger alkali cations.[37] At higher temperatures, 1100−1200 °C, the pyrochlore impurities were reduced but not eliminated. However, no SHG signal was observed in this mixture, indicating that the materials are centrosymmetric. All of the reported materials formed as white, air- and moisture-stable polycrystalline powders.

Structural Characterization. Powder X-ray diffraction data were collected using a PANalytical X'Pert PRO diffractometer equipped with Cu Kα radiation. The 2θ range was 10−120° with a step size of 0.008° and a fixed time of 0.3 s. Rietveld refinement was performed using the *GSAS* program.[38] The archetypal HTBs are often observed in the hexagonal space groups $P6_3/mcm$, $P6_3$, or $P6_322$.[28,39,40] The reported materials have an orthorhombic structure with $a = 3a_h$, $b = \sqrt{3}a_h$, and $c = c_h$, where a_h and c_h are the hexagonal unit cell parameters. The structural refinement of three compounds was carried out in the space group *Cmm*2 (No. 35) with a starting model similar to the single-crystal structure of $Rb_{0.298}Nb_{0.436}W_{0.564}O_3$.[41] We did not observe any crystallographic ordering between the M^{5+} (Nb^{5+} or Ta^{5+}) and W^{6+} cations. Thus, the cations were statistically disordered over the four metal sites, with occupancies fixed such that M^{5+}:W^{6+} = 0.333:0.667. The resulting formulas are in good agreement with the reported stoichiometry. The experimental, calculated, and difference plots for all three compounds, as well as their atomic coordinates and thermal parameters, have been deposited in the Supporting Information. A summary of the crystallographic data for the materials reported in this paper is given in Table 1.

Table 1. Summary of Crystallographic Data and Refinement Results for $KNbW_2O_9$, $RbNbW_2O_9$, and $KTaW_2O_9$

compound	$KNbW_2O_9$	$RbNbW_2O_9$	$KTaW_2O_9$
space group	*Cmm*2	*Cmm*2	*Cmm*2
a (Å)	21.9554(2)	22.00985(12)	22.0025(2)
b (Å)	12.60725(15)	12.66916(7)	12.68532(14)
c (Å)	3.87748(3)	3.8989(2)	3.84456(4)
V (Å^3)	1073.273(13)	1086.182(10)	1073.05(2)
Z	6	6	6
R_p (%)	5.79	5.26	6.31
R_{wp} (%)	8.22	7.83	9.21

Thermogravimetric Analysis (TGA). TGA was carried out on a TGA 2050 thermogravimetric analyzer (TA instruments). The samples were placed in a platinum crucible and heated in oxygen at a rate of 5 °C min^{-1} to 1000 °C.

Dielectric Measurements. Variable-temperature (25−400 °C) dielectric measurements were performed by using a Linkam THMSE600 hot stage. Samples were pressed into pellets (12 mm diameter and ∼1 mm thickness) and sintered at 900−1050 °C for 24 h. Gold paste was applied to both sides of the pellet and cured at 350 °C for 3 h.

SHG. Powder SHG measurements were performed on a modified Kurtz-NLO system[42] using a pulsed Nd:YAG laser with a wavelength of 1064 nm. A detailed description of the equipment and methodology has been published.[43,44] Because the SHG efficiency has been shown to depend strongly on the particle size, polycrystalline samples were ground and sieved into distinct particle size ranges (<20, 20−45, 45−63, 63−75, 75−90, and >90 μm). To make relevant comparisons with known SHG materials, crystalline SiO_2 and $LiNbO_3$ were also ground and sieved into the same particle size ranges. No index matching fluid was used in any of the experiments.

Piezoelectric Measurements. Converse piezoelectric measurements were performed using a Radiant Technologies RT66A piezoelectric test system with a TREK (model 609E-6) high-voltage amplifier, Precision Materials Analyzer, Precision High Voltage Interface, and MTI 2000 Fotonic Sensor. The reported materials were pressed into 12-mm-diameter and ∼0.5-mm-thick pellets. Silver paste was applied to both sides of the pellet surfaces for electrodes. A maximum voltage of 500 V was applied to the samples.

Pyroelectric Measurements. The polarization was measured on a Radiant Technologies RT66A Ferroelectric Test System with a TREK high-voltage amplifier between room temperature and 175 °C in Delta 9023 environmental test chamber. The unclamped pyroelectric coefficient, defined as d*P*/d*T* (change in the polarization with respect to the change in temperature), was determined by

(30) Isupov, V. A.; Agranovskaya, A. I.; Bryzhina, M. F. *Kristallografiya* **1963**, *8*, 108.
(31) Yanovskii, V. K.; Voronkova, V. I.; D'Yakov, V. A. *Kristallografiya* **1976**, *21*, 976.
(32) Yanovskii, V. K.; Voronkova, V. I.; Klimova, I. P. *Ferroelectrics* **1983**, *48*, 239.
(33) Maczka, M.; Hanuza, J.; Kojima, S.; Majchrowski, A.; Van der Maas, J. H. *J. Raman Spectrosc.* **2001**, *32*, 287.
(34) Maczka, M.; Souza Filho, A. G.; Freire, P. T. C.; Mendes Filho, J.; Kojima, S.; Hanuza, J.; Majchrowski, A. *J. Raman Spectrosc.* **2003**, *34*, 199.
(35) Specht, R. W.; Brunner, D. G.; Tomandl, G. *Adv. Ceram. Mater.* **1987**, *2*, 789.
(36) Kar, T.; Choudhary, R. N. P. *Mater. Sci. Eng., B* **2002**, *B90*, 224.
(37) Oi, J.; Kishimoto, A.; Kudo, T. *J. Solid State Chem.* **1993**, *103*, 176.
(38) Larson, A. C.; Von Dreele, R. B. Thesis, Los Alamos National Laboratory, Los Alamos, NM, 1987.
(39) Prinz, H.; Mueller, U.; Ha-Eierdanz, M.-L. *Z. Anorg. Allg. Chem.* **1992**, *609*, 95.
(40) Brusetti, R.; Mueller, U.; Ha-Eierdanz, M.-L. *J. Solid State Chem.* **2003**, *172*, 148.
(41) Mattes, R.; Leimkuhler, M.; Nagel, A. *Z. Anorg. Allg. Chem.* **1990**, *582*, 131.
(42) Kurtz, S. K.; Perry, T. T. *J. Appl. Phys.* **1968**, *39*, 3798.
(43) Porter, Y.; Ok, K. M.; Bhuvanesh, N. S. P.; Halasyamani, P. S. *Chem. Mater.* **2001**, *13*, 1910.
(44) Ok, K. M.; Bhuvanesh, N. S. P.; Halasyamani, P. S. *J. Solid State Chem.* **2001**, *161*, 57.

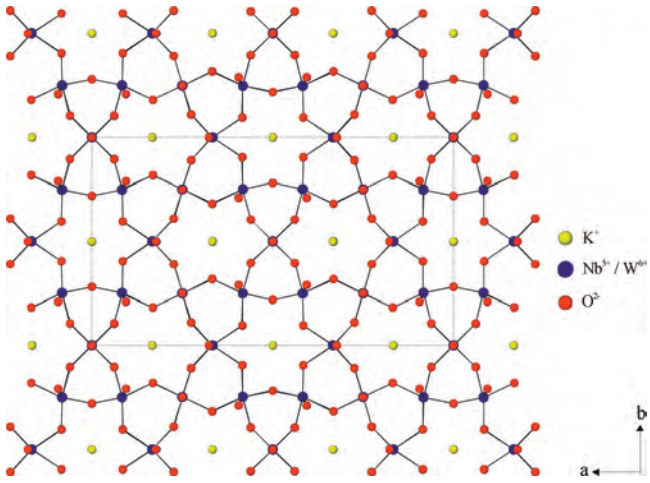

Figure 3. Ball-and-stick diagram of $KNbW_2O_9$ in the *ab* plane. Note that the alkali metal resides in the hexagonal channels.

measuring the polarization as a function of the temperature. The sample was a sintered $^1/_2$-in.-diameter disk (>95% dense) approximately 0.7−0.9 mm thick. Silver paste was applied to both sides. The polarization was measured statistically from room temperature to 175 °C in 20 °C increments, with an electric field of 7−10 kV cm^{-1}. The temperature was allowed to stabilize before the polarization was measured.

Ferroelectric Measurements. All of the samples were sintered $^1/_2$-in.-diameter and approximately 0.5−0.9-mm-thick pellets with conducting silver paste applied to both sides. Ferroelectric hysteresis loops were measured on a Radiant Technologies RT66A Ferroelectric Test System with a TREK high-voltage amplifier. A maximum electric field of 20 kV cm^{-1} was applied to the samples. A frequency of 10 Hz was used during the measurements.

Results

Structure. The crystal structures of the reported materials were determined by laboratory powder X-ray diffraction data. Crystallographic data and refinement results are summarized in Table 1. The reported materials are isostructural, crystallizing in the NCS and polar orthorhombic space group *Cmm*2 (No. 35). The compounds exhibit three-dimensional structures consisting of a corner-shared MO_6 (M = Nb/W or Ta/W) octahedral framework that forms "hexagonal" channels. The alkali cations, K^+ and Rb^+, occupy these channels (see Figure 3). In each structure, there are four unique d^0 cation sites, with each site statistically disordered between Nb^{5+} and W^{6+} or between Ta^{5+} and W^{6+}. No evidence for ordering was observed in the diffraction data. Each of the four unique d^0 transition metals is displaced from the center of their oxide octahedron, resulting in a range of M−O bonds. As we will demonstrate, the magnitude and direction of these intraoctahedral distortions influence the "acentric" properties observed in the materials.

TGA. All of the reported materials are stable up to 1000 °C, as indicated by TGA. The TGA plots for the reported materials have been deposited in the Supporting Information.

Dielectric Measurements. The changes in the dielectric constant for all of the as-prepared materials were measured at variable temperatures (25−400 °C) and frequencies (100 kHz and 1 MHz). The plots of the dielectric permittivity versus temperature for the reported materials have been deposited in the Supporting Information. No dielectric maxima were observed in any of the materials below 400 °C, the maximum temperature of our instrumentation.

"Acentric" Measurements. All of the reported materials crystallize in the NCS and polar orthorhombic space group *Cmm*2. This space group exhibits the correct symmetry for a variety of "acentric" properties including SHG, piezoelectricity, pyroelectricity, and ferroelectricity.

SHG. Powder SHG measurements on the reported materials revealed SHG efficiencies ranging from 180 to 220 × α-SiO_2. We also determined the type 1 phase-matching behavior of the materials by measuring the SHG as a function of the particle size (20−120 μm). In doing so, we were able to calculate $\langle d_{eff} \rangle$, the bulk SHG efficiency, for each material. The phase-matching curves for all of the reported materials have been deposited in the Supporting Information.

Piezoelectric Measurements. Converse piezoelectric measurements were performed on the reported materials. With these measurements, a voltage is applied to the sample that results in a macroscopic deformation. A maximum voltage of 500 V was applied to the samples. For each sample, 20 measurements were performed and an average was taken. The piezoelectric charge constant, d_{33}, was calculated from

$$\Delta L = SL_0 \sim Ed_{33}L_0$$

where ΔL is the displacement of the sample, L_0 is the sample thickness (m), S is the strain ($\Delta L/L_0$), and E is the electric field strength (V m^{-1}). We estimate d_{33} values of 41, 13, and 10 pm V^{-1} for $KNbW_2O_9$, $RbNbW_2O_9$, and $KTaW_2O_9$, respectively. Plots of the piezoelectric data have been deposited in the Supporting Information.

Pyroelectric and Ferroelectric Measurements. The pyroelectric and ferroelectric properties of the materials were determined using the same instrument. Because all of the materials are ferroelectric, the pyroelectric coefficient was determined by measuring the temperature dependence of the remanent polarization. The total pyroelectric coefficient, p^T, at 330 K for $KNbW_2O_9$, $RbNbW_2O_9$, and $KTaW_2O_9$ is −34.5, −6.5, and −9.9 μC m^{-2} K^{-1}, respectively. Ferroelectric measurements were also performed. Hysteresis curves were observed for all of the reported materials. Spontaneous polarization, P_s, values for $KNbW_2O_9$, $RbNbW_2O_9$, and $KTaW_2O_9$ are 8.4, 2.1, and 4.9 μC cm^{-2}, respectively. The pyroelectric and ferroelectric data have been deposited in the Supporting Information.

All of the "acentric" data for the reported materials are given in Table 2.

Discussion. The reported materials, $KNbW_2O_9$, $RbNbW_2O_9$, and $KTaW_2O_9$, are isostructural consisting of MO_6 (M = Nb^{5+}/W^{6+}) octahedra that form a three-dimensional topology. It should be noted again that the M^{5+} and W^{6+} cations are statistically disordered 0.33:0.67 on all of the metal sites. The MO_6 octahedra are corner-shared, with their connectivity resulting in "hexagonal channels" where the alkali metals are observed (see Figure 3). In connectivity terms, the structure may be written as $3[MO_{6/2}]^{1/3-}$, with the charge balance retained by the K^+ or Rb^+ cation. The M−O bond distances range from 1.85(8) to 2.33(3) Å. Attributable

Table 2. SHG, Piezoelectric, Pyroelectric, and Ferroelectric Data for $KNbW_2O_9$, $RbNbW_2O_9$, and $KTaW_2O_9$

compound	SHG efficiency PM/NPM[a]	$\langle d_{eff} \rangle$ converse	piezoelectric coefficient d_{33} (pm V^{-1})	pyroelectric coefficient, p^T ($\mu C\ m^{-2}\ K^{-1}$)	spontaneous polarization P_s ($\mu C\ cm^{-2}$)
$KNbW_2O_9$	220 (NPM)	17.1	41	−34.5	8.4
$RbNbW_2O_9$	190 (NPM)	15.8	13	−6.5	2.1
$KTaW_2O_9$	180 (PM)	7.41	10	−9.9	4.8

[a] PM = phase-matchable. NPM = non-phase-matchable.

Table 3. Magnitude, d^2 (Å^2), of Distortion and Direction for $KNbW_2O_9$, $RbNbW_2O_9$, and $KTaW_2O_9$

	d^2 (Å^2)			
	$KNbW_2O_9$	$RbNbW_2O_9$	$KTaW_2O_9$	direction
M1	0.16	0.15	0.07	vertex
M2	0.04	0.05	0.03	vertex
M3	0.15	0.15	0.06	edge
M4	0.01	0.01	0.00	vertex, $KNbW_2O_9$, $RbNbW_2O_9$; no distortion, $KTaW_2O_9$

to SOJT effects,[20−27] the four unique octahedrally coordinated d^0 cations are asymmetrically bonded to six oxygen atoms. We can quantify the direction and magnitude of these distortions by using continuous symmetry measures and the *Shape* program.[45−48] The results are given in Table 3. The magnitude of the d^0 cation distortion is given as d^2 and in units of Å^2. As can be observed from Table 3, there is a marked decrease in the magnitude of the distortion between $KNbW_2O_9$ and $KTaW_2O_9$. For example, the magnitudes of the distortions for M1 and M2 in $KNbW_2O_9$ are 0.16 and 0.04 Å^2, respectively, whereas for $KTaW_2O_9$, the corresponding values are 0.07 and 0.03 Å^2. Similar decreases are observed with M3 and M4. This is consistent with our earlier observation that octahedrally coordinated Nb^{5+} displaces, on average, to a greater extent than Ta^{5+}.[49] As expected the d^0 cation distortions between $KNbW_2O_9$ and $RbNbW_2O_9$ are very similar. The magnitudes of all of the distortions are consistent with earlier observations.[49] With respect to the direction of the displacements, corner- or vertex-type (local C_4 direction) distortions are observed for M1, M2, and M4. For these cations, there are one "short" bond and one "long" M−O bond trans to each other, with four "normal" M−O bonds. An edge-type (local C_2 direction) distortion is observed for M3, with two "short", two "long", and two "intermediate" M−O bonds. Because the cations are disordered, it is difficult to make precise statements regarding the direction of the distortions. It should be noted, however, that vertex- and edge-type displacements are commonly observed for Nb^{5+}, Ta^{5+}, and W^{6+}.[49]

With the distortions, we must examine not only the local distortions but also the net direction of the polarization. Because the reported materials are isostructural, we will only describe in detail the local and macroscopic polarization in $KNbW_2O_9$. Figure 4 shows the four unique octahedrally coordinated metal cations in $KNbW_2O_9$. The arrows represent the approximate direction of the cation distortion and polarization. As seen in Figure 4, M1, M2, and M4 distort toward a corner, whereas M3 displaces toward an edge. We must also examine how these polarizations "interact"; that is, do they constructively or destructively "interfere" with each other with respect to the three-dimensional crystal structure? Groups of MO_6 octahedra are shown in Figure 5. As can be seen, M1, M2, and M4 form chains that propagate along the c axis. The arrows represent the local and net direction of the polarization. The net direction of the polarization for M1 is toward the $-c$ axis, whereas for M2 and M4, the net polarizations are toward the $+c$ axis. The M3 cation is found in "double octahedral chains". As seen in Figure 5, even though each M3 cation distorts toward an edge, the net polarization resulting from these distortions is zero because all of the polarizations cancel. Returning to the M1, M2, and M4 cations, we note that, although the net polarizations are in opposite directions (M1 toward the $-c$ axis and M2 and M4 toward the $+c$ axis), the total polarization resulting from all of the distortions is toward the $-c$ axis. This is because the distortions associated with M1 are larger than those of M2 and M4 combined. Thus, the net polarization for all three materials is toward the $-c$ axis. Because we know the local and net polarization magnitudes for all of the metal cations, we can begin to develop structure−property relationships. Although there is a decrease in the magnitude of the polarization between $KNbW_2O_9$ and $KTaW_2O_9$, there is only a slight decrease in the measured physical properties (see Table 2). For example, the SHG efficiency for $KNbW_2O_9$ compared with $KTaW_2O_9$ is 220 versus 180 × α-SiO_2, respectively, and spontaneous

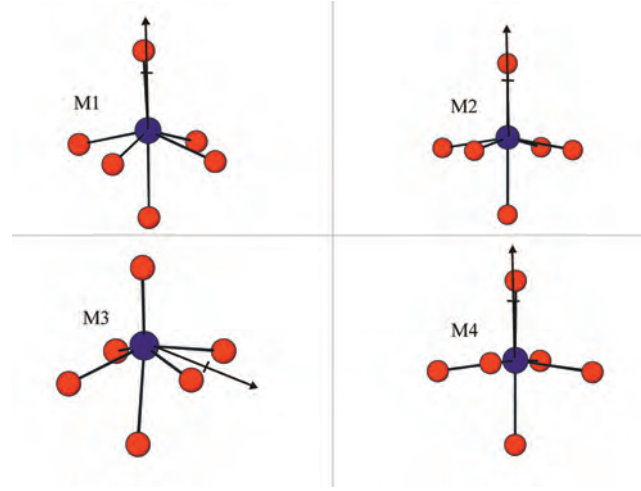

Figure 4. Intraoctahedral distortions in the four unique metal cations in $KNbW_2O_9$. The arrows represent the approximate directions of the distortion and polarization.

(45) Zabrodsky, H.; Peleg, S.; Avnir, D. *J. Am. Chem. Soc.* **1992**, *114*, 7843.
(46) Alvarez, S.; Avnir, D.; Llunell, M.; Pinsky, M. *New J. Chem.* **2002**, *26*, 996.
(47) Alvarez, S.; Alemany, P.; Avnir, D. *Chem. Soc. Rev.* **2005**, *34*, 313.
(48) Llunell, M.; Casanova, D.; Cirera, J.; Bofill, J. M.; Alemany, P.; Alvarez, S.; Pinsky, M.; Avnir, D. *Shape Program*, version 1.1b; University of Barcelona: Barcelona, Spain, 2004.
(49) Ok, K. M.; Halasyamani, P. S.; Casanova, D.; Llunell, M.; Alemany, P.; Alvarez, S. *Chem. Mater.* **2006**, *18*, 3176.

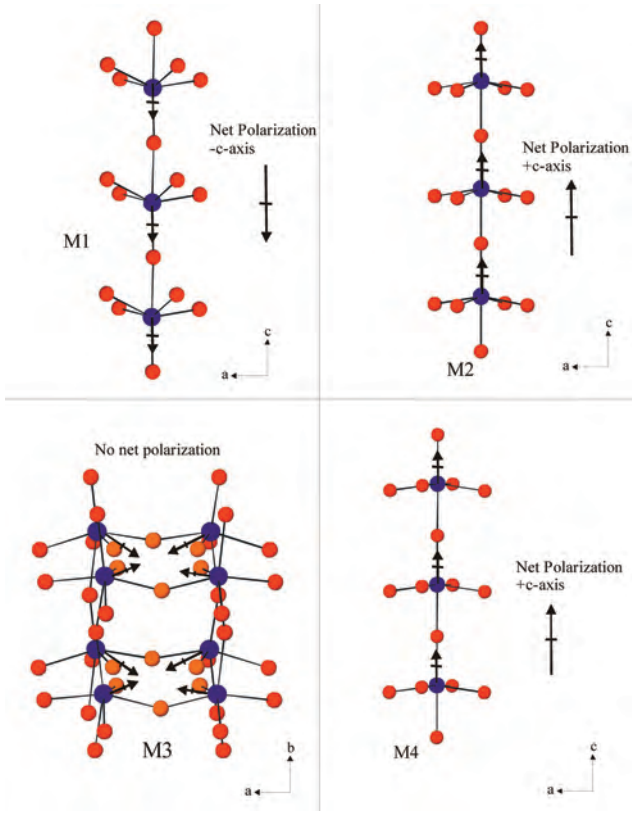

Figure 5. Net polarizations for the four unique metal cations in $KNbW_2O_9$. Note that M1, M2, and M4 have a net polarization along the $\pm c$ axis, whereas M3 generates no net polarization. Note that for M3 the two oxygen atoms that form the "short" M−O bonds are orange.

polarization, P_s, values are 8.4 and 4.8 μC cm^{-2}, respectively. Between $KNbW_2O_9$ and $RbNbW_2O_9$, the magnitudes of the physical properties are similar, although P_s for $RbNbW_2O_9$ is surprisingly small, 2.1 μC cm^{-2}. It is likely that the relatively small piezoelectric, pyroelectric, and ferroelectric responses are attributable to the cancelation of many of the local polarizations.

All of the reported oxides represent functional inorganic materials. The functionality, e.g., SHG, ferroelectric behavior, etc., and its magnitude are intimately tied to the chemical bonding. It is of great importance to understand how the various bonding interactions influence the functionalities. Clearly, SOJT effects on octahedrally coordinated d^0 cations result in distortions that produce local dipole moments. The interaction of these local moments to produce a net polarization in the structure directly determines the magnitude of the "acentric" physical property. Controlling these local moments, in order to maximize the desired physical property, remains an ongoing challenge for synthetic chemists.

Acknowledgment. We thank the Robert A. Welch Foundation, the NSF (Grant DMR-0652150), the ACS-PRF (47345-AC10), and the Texas Center for Superconductivity for support.

Supporting Information Available: X-ray diffraction data (calculated, experimental, and difference), TGA data, dielectric permittivity versus temperature data, SHG phase-matching plots, pyroelectric measurements, ferroelectric hysteresis loops, and atomic coordinates and bond lengths for $KNbW_2O_9$, $RbNbW_2O_9$, and $KTaW_2O_9$. This material is available free of charge via the Internet at http://pubs.acs.org.

IC800573K